

INTERNATIONAL SOCIETY FOR SOIL MECHANICS AND GEOTECHNICAL ENGINEERING



This paper was downloaded from the Online Library of the International Society for Soil Mechanics and Geotechnical Engineering (ISSMGE). The library is available here:

<https://www.issmge.org/publications/online-library>

This is an open-access database that archives thousands of papers published under the Auspices of the ISSMGE and maintained by the Innovation and Development Committee of ISSMGE.

Comparison of effects of complex initial stress state parameters on undisturbed loess dynamic properties

Y. Luo

College of Water Resources and Architectural Engineering, Northwest A&F University, Yangling, China

Z. Wang

College of Water Resources and Architectural Engineering, Northwest A&F University, Yangling, China

Currently at Institute of Geotechnical Engineering, RWTH Aachen University, Aachen, Germany

H. Guo

College of Water Resources and Architectural Engineering, Northwest A&F University, Yangling, China

ABSTRACT: The foundation soil masses under buildings and structures are always in complex initial stress states. Although numerous studies have been conducted on the influences of the complex initial stress state parameters on loess dynamic properties, the influences of those parameters are rarely compared. This study focuses on the comparison of the influences of those parameters (i.e. the angle of initial principal stress α_0 , the coefficient of initial intermediate principal stress b_0 , the initial deviatoric stress ratio η_0 and the initial average principal stress p_{m0}) on loess dynamic properties in China through laboratory testing. The results show that the effects of p_{m0} on the maximum dynamic shear modulus G_0 and the maximum dynamic shear stress τ_{dmax} are similar to the effects of the confining stresses. G_0 and τ_{dmax} decrease with the increment of α_0 . G_0 increases while τ_{dmax} decreases with the increment of η_0 . Among the three parameters (α_0 , b_0 and η_0), α_0 causes the largest differences of G_0 , whilst η_0 causes the largest differences of τ_{dmax} . Therefore, α_0 and η_0 should be given priority to the dynamic response analysis and anti-seismic design of the projects in loess areas.

1 INTRODUCTION

As a kind of special soil with unique structural properties (Gao 1988), loess is widely distributed in the central and western areas of China, where earthquakes happen frequently and fiercely (Lin & Liang 1980, Yuan & Wang 2009). Loess dynamic characteristic parameters are the essential parameters to the foundational dynamic response analysis and the anti-seismic design in those areas. Therefore, obtaining accurate and reasonable designing parameters will highly influence the safety and economy of the project structures in loess areas (Zhou & Chen 2005).

In order to investigate the influencing factors and their effects on loess dynamic properties, numerous studies on water contents, confining pressures, structural properties and regional distributions have been carried out (Luo & Tian 2005, Wang et al. 2010). However, the foundation soil masses of practical projects are always in complex initial stress states, for example, the directions of initial principal stress rotations, the values of initial intermediate principal stresses may change as well as the values of initial deviatoric stresses (Ishihara & Towhata 1983, Oger et al. 1998, Blanc et al. 2011). Therefore, it is important to

investigate the effects of complex initial stress state parameters (the angle of initial principal stress α_0 , the coefficient of initial intermediate principal stress b_0 , the initial deviatoric stress ratio η_0 and the initial average principal stress p_{m0}) on loess dynamic properties.

Wang et al. (2012, 2013) investigated the influences of initial angles of principal stresses and initial deviatoric stress ratios on loess dynamic properties, and they pointed out that the capacities of resisting shear deformations of loess were decreasing with the increase of the initial angles of principal stresses or with the increase of the initial deviatoric stress ratios. Wang et al. (2011) also studied the influences of complex initial stress state parameters on the dynamic shear modulus and dynamic shear strain relations. However, the influences of different complex initial stress state parameters on loess dynamic characteristics are various, which have not been fully investigated in the previous studies. Therefore, this study aims to compare the effects of different complex initial stress state parameters on loess dynamic properties and to provide more accurate and reasonable guiding references for the safety and economy of the project in the engineering design in loess areas.

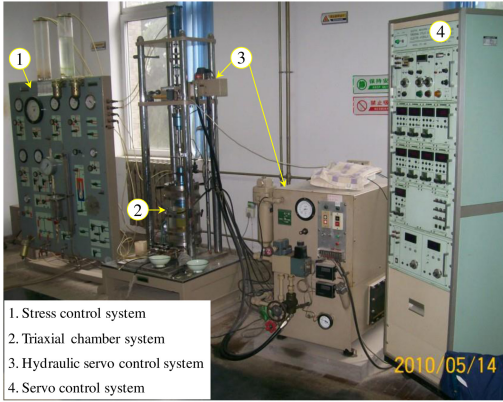


Figure 1. Remodeled DTC-199 torsional cyclic load triaxial apparatus.

2 MATERIALS AND METHODS

2.1 Testing apparatus and soil samples

The experiments were carried out using the remodeled DTC-199 torsional cyclic load triaxial apparatus, as shown in Figure 1. Detailed information about the apparatus has been illustrated in the previous paper (Wang et al. 2012). The soil samples were taken from a typical loess area in Shaanxi Province, China. The natural water content was 19% and the dry density was 1.52 g/cm^3 . Other physical indexes and particle size distribution of the soil can be found in Wang et al. (2012). The testing specimens were all undisturbed hollow cylindrical specimens, which were prepared from natural loess samples using special trimming equipments. Detailed specimen preparation process has been illustrated in the previous paper (Wang et al. 2012). The dimensions of the specimens were: height 100 mm, external diameter 70 mm and internal diameter 30 mm. Laboratory tests with identical specimen sizes as in this study have been conducted on saturated soft clay and silt, respectively (Luan et al. 2010, Guo et al. 2012). In order to reduce the individual differences of the undisturbed specimens, the weights of the specimens should be $568 \pm 8 \text{ g}$. Hence, the corresponding dry densities of the specimens were in the range of $1.50\text{--}1.54 \text{ g/cm}^3$.

2.2 Testing procedures

After installing a specimen, the external pressure p_{e0} and the internal pressure p_{i0} were exerted on the outer and the inner vertical surfaces of the specimen by two membranes, respectively. Meanwhile, the axial force W_0 was applied on the top surface of the specimen. After the specimen reaching the equilibrium state (the vertical deformation of the specimen was less than 0.01 mm/hour), the initial torsion moment M_{T0} was exerted on the top surface of the specimen, which was along the center axis of the specimen. After the specimen reaching the equilibrium state again, the torsional

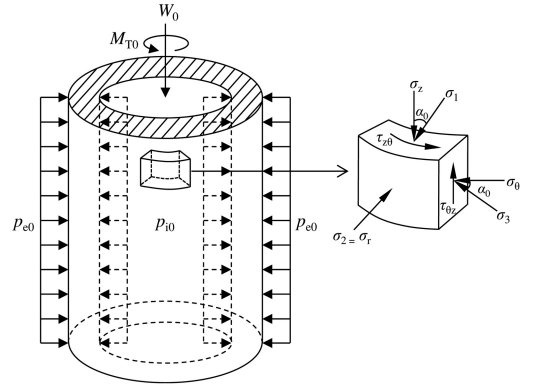


Figure 2. Hollow cylinder specimen and its element's stress states.

Table 1. Experimental schemes.

$\alpha_0/^\circ$	$b_0/-$	$\eta_0/-$	p_{m0}/kPa
0, 30, 45, 60, 90	0.5	0.43	50, 100, 150
45	0, 0.25, 0.5, 0.75, 1	0.43	50, 100, 150
45	0.5	0, 0.43, 0.75, 1	50, 100, 150

Note: $w = 19\%$, $\rho_d = 1.52 \text{ g/cm}^3$.

cyclic load was applied on the top surface of the specimen and the cyclic load increased step by step until the specimen failed or the measured scope of the apparatus was out of the maximum scope. During the testing process, the data such as the dynamic shear stresses and dynamic shear strains were recorded by the corresponding data logger. The testing frequency was 1 Hz and a sine wave was used (Zhou & Chen 2005). All the processes were conducted under undrained conditions.

2.3 Specimen stress states and experimental scheme

The complex initial stress states with the corresponding controlling parameters (α_0 , b_0 , η_0 and p_{m0}) were formed through applying the confining pressures on the inner and outer vertical surfaces, axial force on the top surface and torsion moment along the center axis of the specimen, respectively, as shown in Figure 2. More detailed illustration about the specimen stress states can be found in Wang et al. (2012). When investigating the influences of the each complex initial stress state parameter (α_0 , b_0 or η_0) on undisturbed loess dynamic properties, the other two controlling parameters were kept constant. All the laboratory tests were conducted under the three different initial average principal stresses: $p_{m0} = 50, 100$ and 150 kPa . The specific experimental scheme is shown in Table 1. All the controlling parameters were chosen according to the references (Nakata et al. 1998, Yoshimine et al. 1998, Guo et al. 2005).

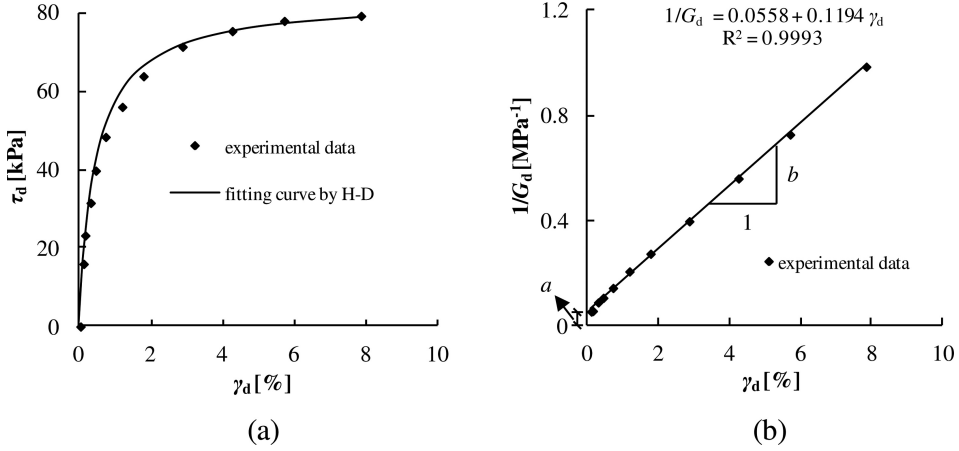


Figure 3. Typical curves of the experimental data based on the Hardin-Drnevich hyperbolic model ($\alpha_0 = 45^\circ$, $b_0 = 0.5$, $\eta_0 = 0.43$, $p_{m0} = 100$ kPa).

3 EXPERIMENTAL RESULTS AND ANALYSES

The effects of the complex initial stress state parameters on the dynamic properties of undisturbed loess have been investigated in previous papers (Wang et al. 2011, Wang et al. 2012, Wang & Luo 2013). This paper aims to compare the effects of different complex initial stress state parameters on loess dynamic properties. The dynamic shear modulus and the damping ratio are the most commonly used parameters to characterize the soil dynamic properties (Biglari et al. 2011, Senetakis et al. 2012, Chaney 2013). However, the dynamic shear modulus and the damping ratio change with changing the dynamic shear strain, the maximum dynamic shear modulus and maximum dynamic shear stress, which are also important parameters of soil dynamic properties (Zhang et al. 2005, El Mohtar et al. 2013), are used in this study. Those two parameters can be obtained from the Hardin-Drevich (H-D) hyperbolic model (Hardin & Drnevich 1972) with the following formulas. Good accordance of the experimental data with the H-D hyperbolic model is shown in Figure 3.

$$\tau_d = \frac{\gamma_d}{\frac{1}{G_0} + \frac{\gamma_d}{\tau_{d\max}}} = \frac{\gamma_d}{a + b \cdot \gamma_d} \quad (1)$$

$$\frac{1}{G_d} = \frac{\gamma_d}{\tau_d} = \frac{1}{G_0} + \frac{\gamma_d}{\tau_{d\max}} = a + b \cdot \gamma_d \quad (2)$$

where: τ_d , γ_d are the dynamic shear stress and the dynamic shear strain, respectively; G_d is dynamic shear modulus; G_0 is the maximum or initial dynamic shear modulus; $\tau_{d\max}$ is the maximum dynamic shear stress; a , b are the intercept and slope of the beeline corresponding to Formula (2), respectively, $a = 1/G_0$, $b = 1/\tau_{d\max}$.

The maximum dynamic shear modulus G_0 and the maximum dynamic shear stress $\tau_{d\max}$ can be computed with $G_0 = 1/a$ and $\tau_{d\max} = 1/b$, respectively.

3.1 Effects of complex initial stress state parameters on maximum dynamic shear modulus

Figure 4 shows the changes of the maximum dynamic shear modulus G_0 with increasing the angle of initial principal stress α_0 , the coefficients of initial intermediate principal stress b_0 and the initial deviatoric stress ratio η_0 , respectively, under different initial average principal stresses p_{m0} . It can be seen that α_0 , b_0 and η_0 have different effects on G_0 : G_0 decreases with increasing α_0 (Figure 4a), while G_0 increases with increasing η_0 (Figure 4c); G_0 fluctuates with increasing b_0 (Figure 4b). It can also be concluded from Figure 4 that the increment of p_{m0} leads to the raise of G_0 . The effects of p_{m0} on G_0 are similar to the effects of the confining stresses on G_0 (Wang et al. 2010). Therefore, this study mainly compares the influences of the other three complex initial stress state parameters (α_0 , b_0 and η_0) on loess dynamic properties.

In order to compare the effects of those three parameters (α_0 , b_0 and η_0) on G_0 , the differences of the maximum and the minimum values of G_0 under various complex initial stress state parameters are summarized in Figure 5. It is possible to observe that, among those three parameters, α_0 causes the largest differences of G_0 under each initial average principal stress p_{m0} , followed by η_0 , and the influence of b_0 is the smallest.

3.2 Effects of complex initial stress state parameters on maximum dynamic shear stress

Figure 6 shows the changes of the maximum dynamic shear stress $\tau_{d\max}$ with the increment of the angle of initial principal stress α_0 , the coefficients of initial intermediate principal stress b_0 and the initial

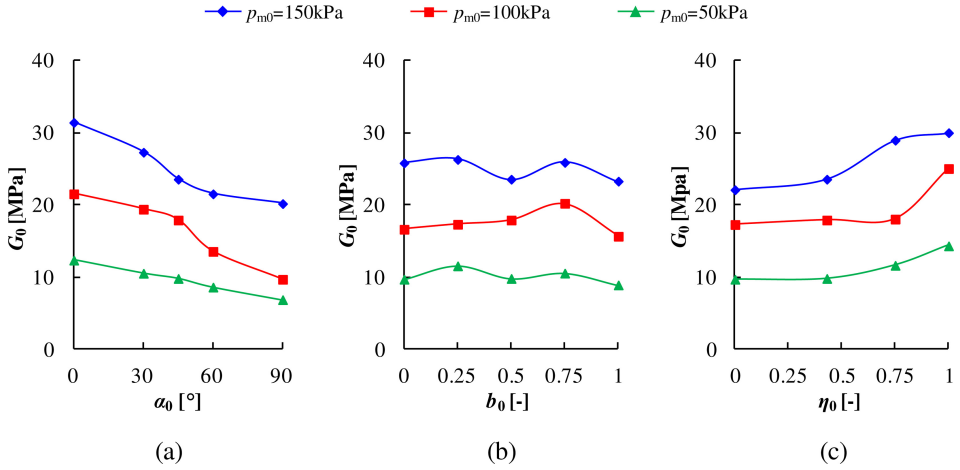


Figure 4. Maximum dynamic shear modulus under different complex initial stress state parameters.

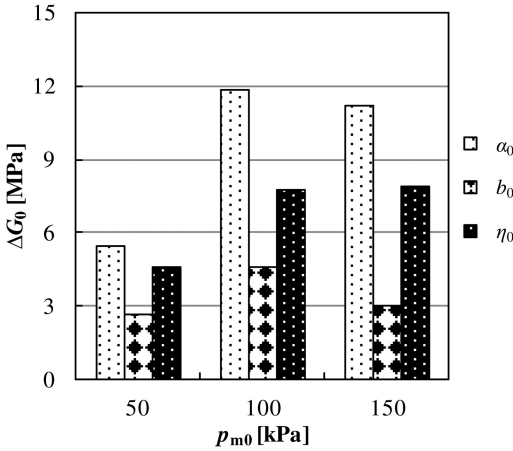


Figure 5. Differences of the maximum and minimum values of G_0 .

deviatoric stress ratio η_0 , respectively, under different initial average principal stresses p_{m0} . τ_{dmax} decreases with increasing α_0 and η_0 , respectively. τ_{dmax} fluctuates with increasing b_0 . Moreover, it is also possible to conclude from Figure 6 that τ_{dmax} increases with increasing p_{m0} although several experimental data are against the total trend.

Similar approaches as the comparison of the effects of those three parameters (α_0 , b_0 and η_0) on G_0 have been used to analyze the influences of those three parameters on τ_{dmax} . The differences of the maximum and the minimum values of τ_{dmax} under various complex initial stress state parameters are summarized in Figure 7. It is possible to observe that, among those three parameters, η_0 causes the largest differences of τ_{dmax} under each initial average principal stress p_{m0} , followed by α_0 , and the influence of b_0 is the smallest. The above correlations are not as clear as the correlations of the differences of G_0 , which might be due

to the slight individual differences of the undisturbed specimens in this study.

4 CONCLUSIONS AND DISCUSSION

The results presented above have led to the following observations:

- (1) The effects of the initial average principal stresses p_{m0} on the maximum dynamic shear modulus G_0 and the maximum dynamic shear stress τ_{dmax} are similar to the effects of the confining stresses on G_0 and τ_{dmax} . More attentions should be paid on the effects of p_{m0} on loess dynamic properties.
- (2) The influences of the angles of initial principal stresses α_0 on the maximum dynamic shear modulus G_0 and the maximum dynamic shear stress τ_{dmax} are similar. G_0 and τ_{dmax} decrease with the increment of α_0 . The reason for such results can be explained by the experimental control parameters and the stress states of the specimens Wang & Luo (2013). When $\alpha_0 = 0^\circ$, the specimen was compacted under the largest axial confining stress; hence, G_0 and τ_{dmax} are the largest. While $\alpha_0 = 90^\circ$, the specimen was stretched under the negative axial confining stress; therefore, G_0 and τ_{dmax} are relatively small compared with those under $\alpha_0 = 0^\circ$. Figure 8 shows the heights of the specimens under different angles of initial principal stresses after testing. The influences of the initial deviatoric stress ratios η_0 on the maximum dynamic shear modulus G_0 and the maximum dynamic shear stress τ_{dmax} , however, are different. G_0 increases while τ_{dmax} decreases with the increment of η_0 . Similar explanations for the results can be found in Wang et al. (2012).
- (3) Further investigation shows that among the three parameters (α_0 , b_0 and η_0), α_0 and η_0 cause the largest differences of G_0 and τ_{dmax} . Therefore, α_0

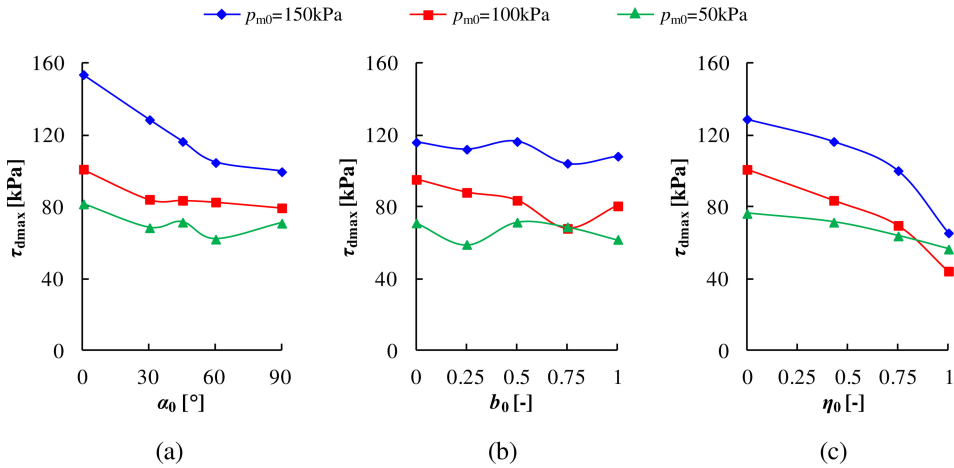


Figure 6. Maximum dynamic shear stresses under different complex initial stress state parameters.

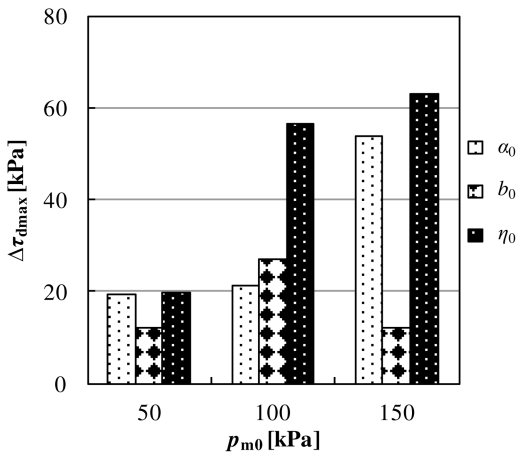


Figure 7. Differences of the maximum and minimum values of τ_{dmax} .



Figure 8. Heights of the specimens under different angles of initial principal stresses (after testing).

and η_0 should be given priority to the dynamic response analysis and anti-seismic design of the projects in loess areas.

The above conclusions are based on the laboratory tests conducted at Northwest A&F University and all the specimens in this study are undisturbed, hence

slight discrepancy might be caused by the individual differences of the samples.

ACKNOWLEDGEMENTS

The work was financially supported by the National Natural Science Foundation of China (No. 50578134) and the program for New Century Excellent Talents of Chinese Ministry of Education (No. NCET-06-0864). The second author appreciates the scholarship from the China Scholarship Council (No. 2010630201).

REFERENCES

- Biglari, M., Jafari, M.K., Shafiee, A., Mancuso, C., & d'Onofrio, A. 2011. Shear modulus and damping ratio of unsaturated kaolin measured by new suction-controlled cyclic triaxial device. *Geotech. Test. J.* 34(5): 525–536.
- Blanc, M., Di Benedetto, H., & Tiouajni, S. 2011. Deformation characteristics of dry Hostun sand with principal stress axes rotation. *Soils Found.* 51(4): 749–760.
- Brennan, A.J., Thusyanthan, N.I., & Madabhushi, S.P.G. 2005. Evaluation of shear modulus and damping in dynamic centrifuge tests. *J. Geotech. Geoenviron. Eng. ASCE* 131(12): 1488–1497.
- Chaney, R. 2013. Dynamic properties of some Eastern Mediterranean marine sediments. *Geotech. Test. J.* 36(4): 524–532.
- El Mohtar, C.S., Drnevich, V.P., Santagata, M., & Bobet, A. 2013. Combined resonant column and cyclic triaxial tests for measuring undrained shear modulus reduction of sand with plastic fines. *Geotech. Test. J.* 36(4): 484–492.
- Gao, G. 1988. Formation and development of the structure of collapsing loess in China. *Eng. Geol.* 25(2–4): 235–245.
- Guo, Y., Luan, M., Shi, D., Xu, C., He, Y., & Li, M. 2005. Experimental study on effect of initial stress condition on dynamic behavior and deformation parameters of loose sands. *Rock Soil Mech.* 26(8): 1195–1200.
- Guo, Y., Zhang, J., Luan, M., & Liu, G. 2012. Effect of orientation of initial principal stress on undrained shear behavior of saturated silt. *Chin. J. Geotech. Eng.* 34(1): 166–171.

- Hardin, B.O. & Drnevich, V.P. 1972. Shear modulus and damping in soils: design equations and curves. *J. Soil Mech. Found. Div. ASCE* 98(7): 667–692.
- Ishihara, K. & Towhata, I. 1983. Sand response to cyclic rotation of principal stress directions as induced by wave loads. *Soils Found.* 23(4): 11–26.
- Lin, Z. & Liang, W. 1980. Distribution and engineering properties of loess and loesslike soils in China. *Bull. Eng. Geol. Environ.* 21(1): 112–117.
- Luan, M., Liu, G., Wang, Z., & Guo, Y. 2010. Stiffness degradation of undisturbed saturated soft clay in the Yangtze estuary under complex stress conditions. *China Ocean Eng.* 24(3): 523–538.
- Luo, Y. & Tian, K. 2005. Dynamic shear modulus and damping ratio of unsaturated loess. *J. Hydraulic Eng.* 36(7): 830–834.
- Lo Presti, D.C.F., Jamiolkowski, M., Pallara, O., Cavallaro, A., & Pedroni, S. 1997. Shear modulus and damping of soils. *Géotechnique* 47(3): 603–617.
- Nakata, Y., Hyodo, M., Murata, H., & Yasufuku, N. 1998. Flow deformation of sands subjected to principal stress rotation. *Soils Found.* 38(2): 115–128.
- Oger, L., Savage, S.B., Corriveau, D., & Sayed, M. 1998. Yield and deformation of an assembly of disks subjected to a deviatoric stress loading. *Mech. Mater.* 27(4): 189–210.
- Senetakis, K., Anastasiadis, A., & Pitilakis, K. 2012. The small-strain shear modulus and damping ratio of quartz and volcanic sands. *Geotech. Test. J.* 35(6): 964–980.
- Wang, Z., Luo, Y., Wang, R., Yang, L., & Tan, D. 2010. Experimental study on dynamic shear modulus and damping ratio of undisturbed loess in different regions. *Chin. J. Geotech. Eng.* 32(9): 1464–1469.
- Wang, Z., Luo, Y., & Guo, H. 2011. Effects of complex initial stress state parameters on dynamic shear modulus of loess. *Adv. Mater. Res.* 243–249: 2601–2606.
- Wang, Z., Luo, Y., Guo, H., & Tian, H. 2012. Effects of initial deviatoric stress ratios on dynamic shear modulus and damping ratio of undisturbed loess in China. *Eng. Geol.* 143–144: 43–50.
- Wang, Z. & Luo, Y. 2013. Effects of initial angles of principal stresses on dynamic deformation properties of loess. *J. Earthq. Eng. Eng. Vib.* 33(1): 184–191.
- Yoshimine, M., Ishihara, K., & Vargas, W. 1998. Effects of principal stress direction and intermediate principal stress on undrained shear behavior of sand. *Soils Found.* 38(3): 179–188.
- Yuan, Z. & Wang, L. 2009. Collapsibility and seismic settlement of loess. *Eng. Geol.* 115(1–2): 119–123.
- Zhang, J., Andrus, R.D., & Juang, C.H. 2005. Normalized shear modulus and material damping ratio relationships. *J. Geotech. Geoenviron. Eng. ASCE* 131(4): 453–464.
- Zhou, Y. & Chen, Y. 2005. Influence of seismic cyclic loading history on small strain shear modulus of saturated sands. *Soil Dyn. Earthq. Eng.* 25(5): 341–353.